Journal of Luminescence 224 (2020) 117289

Contents lists available at ScienceDirect

Journal of Luminescence

journal homepage: http://www.elsevier.com/locate/jlumin

Atomic deciphering of cation exchange mechanism in upconversion nanoparticles

Ming Guan [a], Maxim S. Molokeev [b,c], Jiajia Zhou [a,*]

[a] UTS-SUStech Joint Research Centre for Biomedical Materials & Devices, Southern University of Science and Technology, Shenzhen, 518055, Guangdong, PR China
[b] Laboratory of Crystal Physics, Kirensky Institute of Physics, SB RAS, Krasnoyarsk, 660036, Russia
[c] Siberian Federal University, 79 Svobodny Ave., Krasnoyarsk, 660041, Russia

ARTICLE INFO

Keywords:
Mn^{2+}
β-$NaYF_4$ nanoparticles
Cation exchange
Rietveld refinement

ABSTRACT

Transition metal ion doping in upconversion nanoparticles (UCNPs) provides an effective way to enhance the luminescence for their wide array of applications. However, the doping sites of transition metal ions have not been comprehensively explored, and commonly assumed that transition metal ions replace the trivalent lanthanides within the lattice. Here we report that cation exchange of transition metal (Mn^{2+}) in β-$NaYF_4$:Yb^{3+}/Er^{3+} UCNPs occurs through alkaline metal (Na^+) replacement, via $2Na^+ \leftrightarrow Mn^{2+} + Vacancy$ reaction. This process distorts the LnF_9 polyhedrons and tailors the surrounding environment around the trivalent lanthanides, thereby improving the upconversion intensity from active lanthanides. Further confirmed by core-shell design and spectroscopic study, we prove that the transition–alkaline metal exchange enables both the emission enhancement and transition probability variation of activators.

1. Introduction

Lanthanide (Ln^{3+}) doped upconversion nanoparticles (UCNPs), featuring by unique luminescent properties including large Stokes shift, tunable emission spectrum and decay lifetime, zero autofluorescence background and high penetration depth into biological tissue, is emerging as a promising light carrier. The UCNPs are attractive in a wide array of applications [1–7], such as graphics imaging and display [8–10], anti-counterfeiting [11,12], and biological labelling [13–17]. In order to expedite the practical applications of UCNPs, great research efforts have been paid to enhance the upconversion luminescence [18–20]. Tailoring the local crystal field of the Ln^{3+} ions could be an effective strategy. Accordingly, many transition metal ions including Li^+ have been introduced into various UCNPs to modulate their upconversion luminescence [21,22]. Hong et al. have reported Zn^{2+} doped $NaYF_4$: Yb^{3+}/Er^{3+} UCNPs and found the improvement of the upconversion luminescence [23]. Kim et al. have successfully incorporated Fe^{3+} ions in β-$NaGdF_4$:Yb^{3+}/Er^{3+} UCNPs, which significantly increased the visible green and red UC emissions [24].

Transition metal Mn^{2+} ion is an interesting species with significantly long lifetime (typically microsecond scale), which has been frequently employed to tune the emission colour or lifetime of $NaLnF_4$ UCNPs [25,26]. However, the emission intensity probably encounters a decline instead due to the direct doping induced phase transition from hexagonal to cubic [27,28]. In contrast, cation exchange is an efficient way to introduce Mn^{2+} ions in UCNPs, with constant morphology and crystal phase compared to initial nanoparticles [29–31]. Liu et al. have reported a cation exchange method and for the first time successfully prepared Mn^{2+}-doped β-$NaGdF_4$ UCNPs, in which Gd host is promoted to assist colour modulation through energy migration [32]. To date, the mechanism of such cation exchange of transition metal ions within $NaYF_4$ UCNPs has not been comprehensively explored. Particularly, it has been generally assumed that the transition metal ions replace the Ln^{3+} instead of Na^+ ions within the lattice of UCNPs. However, because of the differences in ionic radius and electronic polarity to the trivalent Ln^{3+} host ions, the Mn^{2+} ions could induce different local substitution in UCNPs.

In this work, we report a successful execution of Mn^{2+} ions cation exchange in β-$NaYF_4$:Yb^{3+}/Er^{3+} UCNPs. We achieve emission intensity enhancement from Y host, and simultaneously this Mn^{2+} ions cation exchange enables red-to-green emission ratio change. We conduct Rietveld refinement to analyse the crystal structure evolution upon exchange, and further link the crystalline analysis to spectroscopic study to decipher the atomic reaction within a nanoparticle. This enables us to clearly understand the exchange process. This suggests a new pathway

* Corresponding author.
E-mail address: Jiajia.Zhou@uts.edu.au (J. Zhou).

https://doi.org/10.1016/j.jlumin.2020.117289
Received 9 December 2019; Received in revised form 11 March 2020; Accepted 11 April 2020
Available online 16 April 2020
0022-2313/© 2020 Elsevier B.V. All rights reserved.

to alter the symmetry of the crystal field around the activator ions, leading to enhanced upconversion.

2. Experimental

$YCl_3{\cdot}6H_2O$ (99.99%), $ErCl_3{\cdot}6H_2O$ (99.99%), $YbCl_3{\cdot}6H_2O$ (99.99%), NH_4F (99.99%), NaOH (98%), 1-octadecene (ODE, 90%), oleic acid (OA, 90%), $MnCl_2$ (99.99%) and hydrochloric acid (HCl, 37%) were purchased from Sigma-Aldrich. Toluene (99.5%), ethanol (100%), methanol (100%), were purchased from Chem-Supply (Australia). All reagents were used as received without further purification.

2.1. Synthesis of β-$NaYF_4$: Yb^{3+}/Er^{3+} UCNPs

A modified synthesis method is adopted to prepare β-$NaYF_4$:40% Yb^{3+}/2%Er^{3+} UCNPs [33]. In a typical procedure, a methanol solution of 0.58 mmol YCl_3, 0.4 mmol $YbCl_3$, and 0.02 mmol $ErCl_3$ was mixed with 6 ml OA and 15 ml ODE in a 50 mL flask. The mixture was heated at 150 °C under stirring until the solution became clear. After cooling to 50 °C, a methanol solution containing NH_4F (4 mmol) and NaOH (2.5 mmol) was added with vigorous stirring for more than 1 h. Then, the mixed solution was heated to 90 °C–150 °C to evaporate all the residual methanol and water. Finally, the solution was heated to 300 °C and kept there for 1.5 h under argon. After washing with cyclohexane/ethanol, the synthesized nanoparticles were dispersed in cyclohexane for use. The core-shell β-$NaYF_4$:40%Yb^{3+}/2%Er^{3+} @$NaYF_4$ UCNPs is obtained via an epitaxial grown shell precursor's layer onto the core UCNPs. The shell precursor is prepared following a similar procedure to that just described in synthesizing the core, except experiencing a reaction at 300 °C.

2.2. Cation exchange of Mn^{2+} ions in β-$NaYF_4$: Yb^{3+}/Er^{3+} UCNPs

Cation exchange of Mn^{2+} ions in $NaYF_4$:Yb^{3+}/Er^{3+} UCNPs are performed according to a previous report [32]. In a typical process, the as-prepared oleic acid-capped nanoparticles were dispersed in a mixed solution of ethanol (1 mL) and HCl (0.2 M; 1 mL). The mixture was sonicated for 5 min and collected by centrifugation. Subsequently, the resulting products were washed with ethanol/water several times and re-dispersed in water. After that, a stock aqueous solution (0.9 ml; 0.05 mmol) of the as-prepared ligand-free $NaYF_4$: Yb^{3+}/Er^{3+} nanoparticles was mixed with an aqueous solution of $MnCl_2$ (0.1 ml). The resulting mixture was shaken thoroughly and heated at 90 °C for 30 min. The products were collected by centrifugation, washed with water several times, and re-dispersed in water. Subsequently, weighing method was used to determine the concentration of UCNPs, and all the UCNPs solution were diluted to the same concentration of 1 mg/ml for testing.

2.3. Characterization

X-ray diffraction (XRD, D8 Advance diffractometer, Bruker Corporation, Germany, with Cu-Kα and linear VANTEC detector, λ = 0.15406 nm, 40 kV, 30 mA) was used to examine the phase composition. The powder diffraction data for Rietveld analysis were collected in the 2θ range of 5∼100° with a step size of 0.02° and counting time of 2∼3 s per step. Rietveld refinement was performed using TOPAS 4.2 software. The morphology of the synthesized nanocrystals was characterized using transmission electron microscopy (TEM; Philips CM10 TEM) at an operating voltage of 100 kV. Elemental analysis was acquired by an energy-dispersive X-ray spectroscopy (EDX). The UC luminescence spectra were obtained using of a Fluorolog-Tau3 spectrofluorometer (JobinYvon-Horiba) equipped with an external 980 nm CW diode laser with a pump power density of 500 W/cm^2. All the measurements were carried out at room temperature.

3. Results and discussion

Fig. 1a illustrates the designed cation exchange synthetic strategy to produce different concentration of Mn^{2+} ions doped β-$NaYF_4$:Yb^{3+}/Er^{3+} UCNPs. Fig. 1b reveals the enhanced UC luminescence properties of these exchanged UCNPs compared to the Mn^{2+}-free sample. We tuned the concentration of $MnCl_2$ during exchange, and labelled the produced UCNPs as Mn^{2+}-less, Mn^{2+}-highly, and Mn^{2+}-ultra-highly doped UCNPs according to 5, 50, and 100 mM Mn^{2+} ions precursors, respectively. Under 980 nm laser excitation, we observed two major UC emission bands in the spectra of all UCNPs. The green emissions centred at 537 and 555 nm originate from the $^2H_{11/2} \rightarrow {}^4I_{15/2}$ and $^4S_{3/2} \rightarrow {}^4I_{15/2}$ transitions of Er^{3+} ions, respectively; the red emission located at 652 nm is attributed to the $^4F_{9/2} \rightarrow {}^4I_{15/2}$ transition of Er^{3+} ions. Clearly, both of the green and red emission of various UCNPs increase with the adding of Mn^{2+} ions from 0 to 50 mM, and subsequently decrease with the continuous increase of Mn^{2+} to 100 mM (Fig. 1c). Under 50 mM Mn^{2+} ions for cation exchange, the sample shows maximum emission intensity, which equals to 2 times as much as the Mn^{2+}-free UCNPs.

To confirm the successful exchange, we performed TEM and elemental analysis to check the morphology and ion distribution change of UCNPs after Mn^{2+} exchange. The Mn^{2+}-free UCNPs show spherical-like morphology and uniform distribution of size (Fig. 2a). After cation exchange by Mn^{2+} ions, the Mn^{2+}-less show negligible changes in terms of crystalline morphology (Fig. 2b), while the size of Mn^{2+}-highly doped β-$NaYF_4$:Yb^{3+}/Er^{3+} UCNPs slightly decrease than the initial NPs (Fig. 2c). Additionally, the elemental mapping result in Fig. 2d shows the presence of Mn element on the surface of UCNPs (note the grey pixels of the image represents the distribution of the Mn^{2+} element). These observations confirm that Mn^{2+} ions successfully penetrated into the surface of UCNPs by cation exchange. To further confirm the entered Mn^{2+} ions locate at the lattice, we performed XRD Rietveld refinement to analyse the crystal structures. In Fig. 2e, all the X-ray patterns are in line with the hexagonal $NaYF_4$, indicating that the particle phase did not change after cation exchange. Rietveld refinements, which take $NaYF_4$ (JCPDS card no. 1517675) as starting model, are stable and give low *R*-factors (Table S1). All thermal parameters show good values (Table S2) and bond distances are in good range (Table S3). In addition, the refined lattice parameters of *a*, *c*, and cell volume of *V* show obvious decreasing trends as a function of Mn^{2+} concentrations (Fig. 2f, Table S1). This is due to the smaller ionic radii of Mn^{2+} in coordinate of CN = 6 (IR = 0.83 Å) compared to Na^+ (IR = 1.02 Å); and smaller ionic radii of Mn^{2+} in coordinate of CN = 8–9, (IR = 0.96 Å, note the maximum coordinate is 8) compared to Y^{3+}(IR = 1.019–1.075 Å), Yb^{3+}(IR = 0.985–1.042 Å), and Er^{3+} (IR = 1.004–1.062 Å). The doping of Mn^{2+} shrinks the unit cells of the UCNPs by replacing Na^+ or Ln^{3+} ions. As we have known, single UCNP is comprised of numerous unit cell, therefore the decreased unit cells induce a slightly decreased size of particles. The decrease of *a*, *c*, and *V* proves that the Mn^{2+} ions have been exchanged into the lattice, yielding Mn^{2+} doped β-$NaYF_4$:Yb^{3+}/Er^{3+} UCNPs.

In order to atomically decipher the exchange process, we analysed the detailed crystal structures and polyhedrons evolution within these UCNPs. The NaF_6 and LnF_9 polyhedral distortion index, *D*, can be calculated as followed:

$$D = \frac{1}{n}\sum_{i=1}^{n}\frac{|l_i - l_{av}|}{l_{av}} \quad (1)$$

where l_i is the distance between central atom and the *i*th coordinating atom, and the l_{av} is the mean bond length [34]. These data were shown in Table S3. Fig. 3a shows the NaF_6 polyhedron within the Mn^{2+}-doped UCNPs. With the increasing of Mn^{2+} concentration, the average Na^+–F^- bond distances show a dramatic decrease trend (2.34 Å→ 2.33 Å→ 2.31 Å) (Fig. 3b), which means that $2Na^+ \leftrightarrow Mn^{2+} + Vacancy$ reaction happens in this crystal system. The replacement of Na^+ by Mn^{2+} induces decrease of the distortion index of (Na/Mn)F_6 polyhedron (5.78 ×

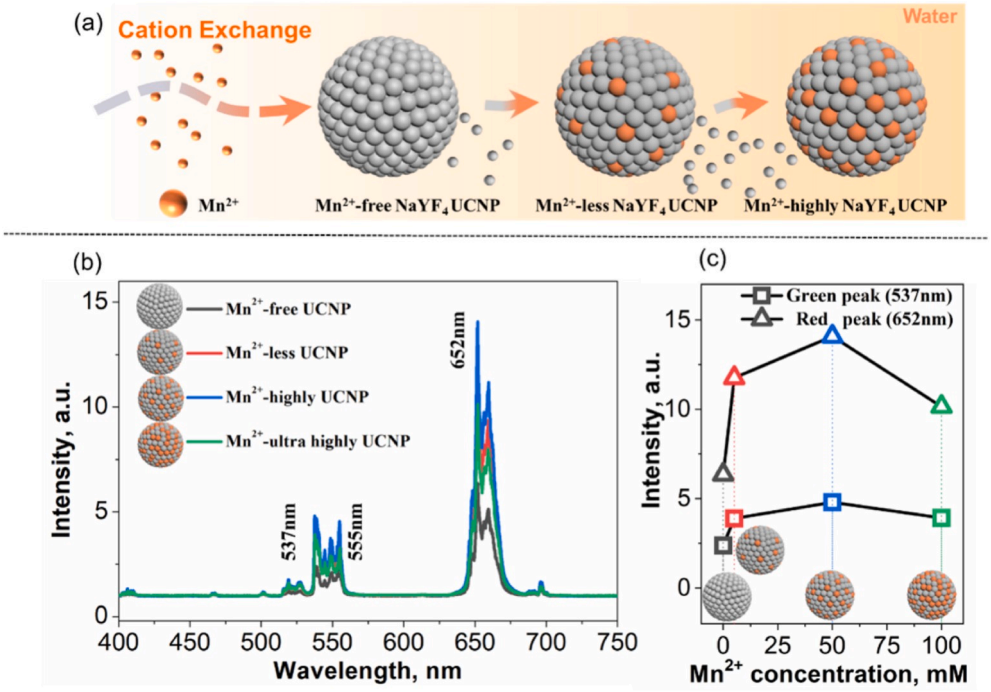

Fig. 1. Schematic showing the cation exchange process to produce Mn^{2+} doped β-$NaYF_4$:Yb^{3+}/Er^{3+} UCNPs with different Mn^{2+} concentrations in a aqueous solution (a); UC emission spectra of as-synthesized Mn^{2+}-free, Mn^{2+}-less, Mn^{2+}-highly, and Mn^{2+}-ultra-highly β-$NaYF_4$:Yb^{3+}/Er^{3+} UCNPs (b); Intensity enhancement for green (537 nm) and red (652 nm) emission as a function of Mn^{2+} concentration (c).

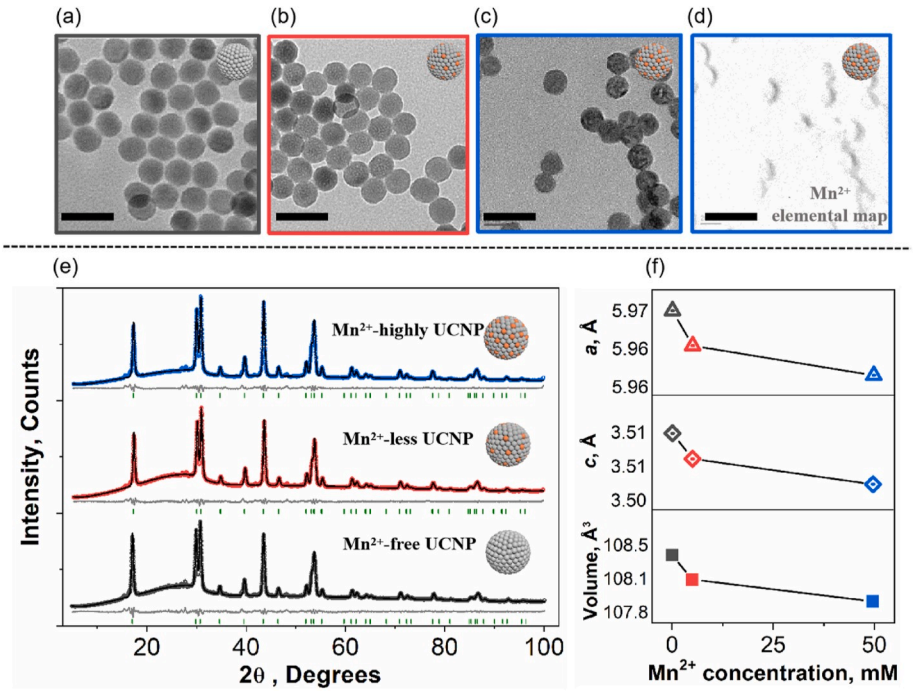

Fig. 2. TEM images before and after cation exchange by Mn^{2+} ions: Mn^{2+}-free (a), Mn^{2+}-less (b) and Mn^{2+}-highly doped β-$NaYF_4$:Yb^{3+}/Er^{3+} UCNPs (c); elemental mapping of the Mn^{2+}-highly doped UCNPs, note the grey pixels represents the concentration of Mn^{2+} element (d); XRD patterns for the refinement of Mn^{2+}-free, Mn^{2+}-less and Mn^{2+}-highly doped UCNPs (e); Refined lattice parameters of a, c, and cell volume (V) showing obvious decreases with increasing Mn^{2+} concentration, indicating Mn^{2+} is doped into the lattice (f). (Scale bar: 50 nm).

10^{-2}→ 5.31 × 10^{-2}→ 5.01 × 10^{-2}) (Fig. 3c). In contrast, the average Ln^{3+}–F^- bond lengths in LnF_9 polyhedron (Fig. 3d) stay almost invariable (2.344 Å→ 2.344 Å→ 2.348 Å) with Mn^{2+} concentration increasing (Fig. 3e), which means that Mn^{2+} less likely to occupy the site of Ln^{3+}. However, the LnF_9 polyhedral distortion enlarges (6.29 × 10^{-3}→ 6.69 × 10^{-3}→ 7.17 × 10^{-3}) with the higher doping of Mn^{2+} ions (Fig. 3f), which indicates Mn^{2+} ions are strongly disordered over crystal and coordinate with LnF_9 polyhedra. In this case, the Mn^{2+} ions doping by cation exchange makes (Na/Mn)F_6 become regular, but the polyhedrons of LnF_9 become more distorted. That is, the $Mn^{2+} \leftrightarrow Na^+$ exchange varies the asymmetric environment, leading to the LnF_9 polyhedral distortion within the lattice of UCNPs. This process tailors the surrounding environment around the Er^{3+} ions in the crystal field, thereby improving the luminescent performance of UCNPs.

The red-to-green emission intensity ratio (I_R/I_G) of Er^{3+} ions is a further evidence of successful incorporation of Mn^{2+} ions in the lattice of

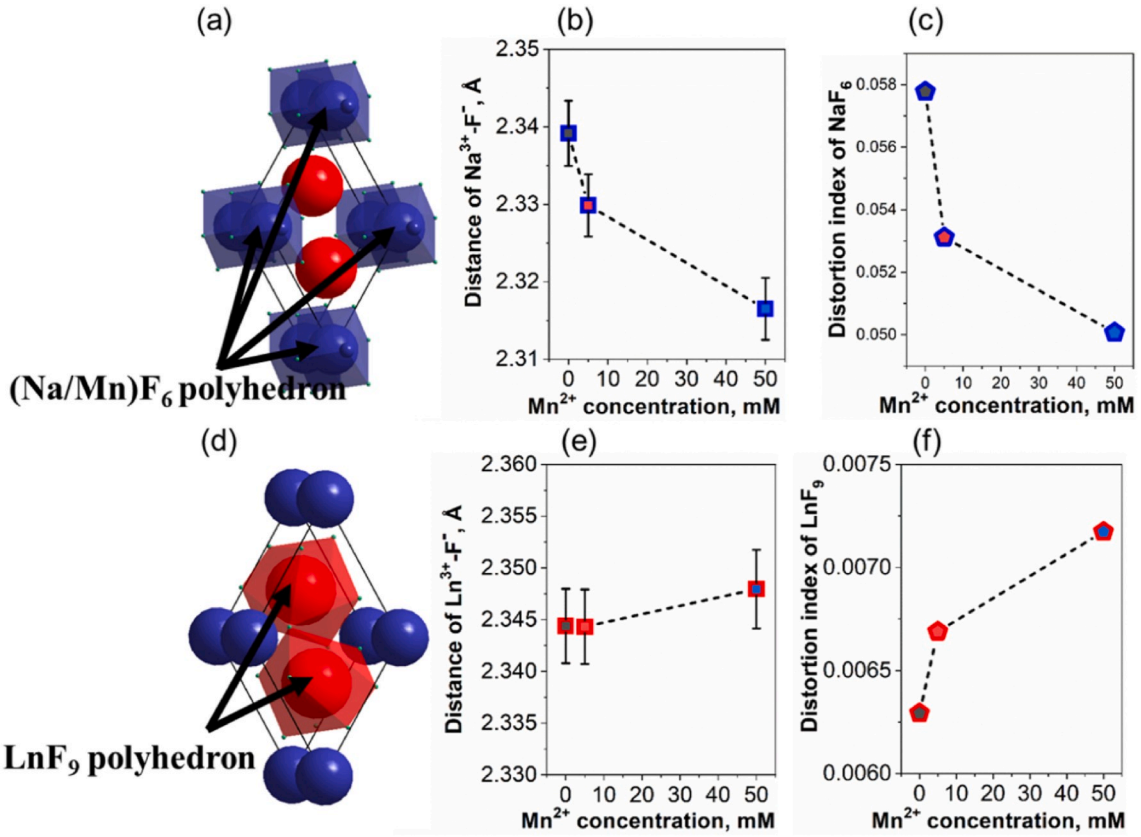

Fig. 3. Schematic showing the lattice structure and the NaF_6 polyhedron within the Mn^{2+}-doped UCNPs (a); Calculated Na^{+}–F^{-} bond distances (b) and NaF_6 polyhedron distortion indexes (c) showing a decrease trend with increasing Mn^{2+} concentration; Schematic showing LnF_9 polyhedron within the Mn^{2+}-doped UCNPs (d); Calculated average Ln^{3+}–F^{-} bond lengths stay almost invariable as a function of Mn^{2+} concentration (e); Enlarged LnF_9 polyhedral distortion with increasing Mn^{2+} concentration (f).

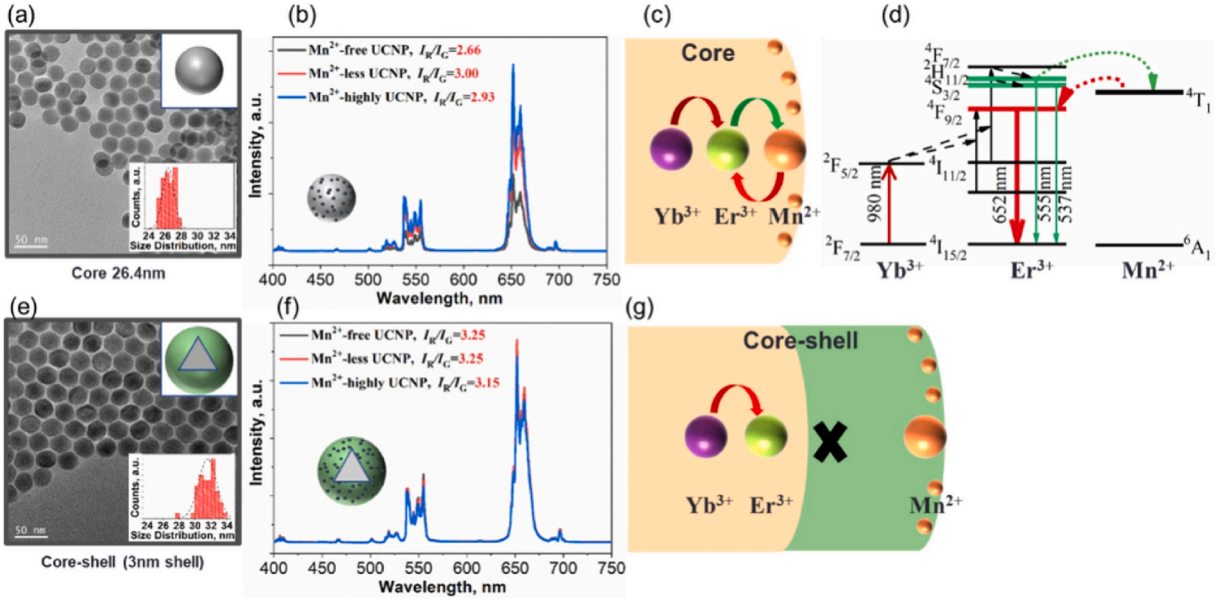

Fig. 4. TEM image and size distribution chart of core β-$NaYF_4$:Yb^{3+}/Er^{3+} UCNPs (a); UC spectra and enhanced red-to-green luminescence ratio (IR/IG) in Mn^{2+}-free, Mn^{2+}-less and Mn^{2+}-highly doped core UCNPs (b); Schematic and energy level diagram showing that Mn^{2+} ions disturbed the transition possibilities and facilitated red emission of Er^{3+} in core UCNPs (c, d); TEM image and size distribution chart of core-shell β-$NaYF_4$:Yb^{3+}/Er^{3+}@ $NaYF_4$ UCNPs with 2.5 nm inert shell (e); UC spectra showing no any I_R/I_G ratio enhancement in Mn^{2+} doped core-shell UCNPs (f); Schematic showing that Mn^{2+} exchanged in 2.5 nm shell are not able to distort the Er^{3+}site occupancy within the polyhedron structure in the core (g).

β-$NaYF_4$:Yb^{3+}/Er^{3+} UCNPs. To clarify it, we designed core-shell $NaYF_4$:Yb^{3+}/Er^{3+}@$NaYF_4$ UCNPs. The core UCNPs have an average size of 24.1 nm (Fig. 4a). The core–shell UCNPs display uniform spherical shape, with an average size of 28.9 nm (Fig. 4e), indicating the inert-shell thickness is about 2.5 nm. After cation exchange by Mn^{2+} ions, the I_R/I_G ratio (652/537 nm) in the core $NaYF_4$: Yb^{3+}/Er^{3+} UCNPs gradually increasing from 2.66 in Mn^{2+}-free UCNPs to 3.00 in Mn^{2+}-less UCNPs (or 2.93 in Mn^{2+}-highly UCNPs), as shown in Fig. 4b. Due to the existence of Mn^{2+} ions in the lattice, the energy from Yb^{3+} sensitizers was transferred from $^2H_{11/2}$ and $^4S_{3/2}$ levels of Er^{3+} to the $^4T_1$ level of Mn^{2+} through nonradiative energy transfer, followed by further back-energy transfer to the $^4F_{9/2}$ level of Er^{3+} [27, 35, 36]. The Mn^{2+} ions change the transition possibilities of Er^{3+}, and finally facilitate the intensity enhancement of the red emission from $^4F_{9/2} \rightarrow {}^4I_{15/2}$ (Fig. 4b, c, d). In contrast, the UC emissions of core-shell $NaYF_4$:Yb^{3+}/Er^{3+}@$NaYF_4$ UCNPs are absence of enhancement after cation exchange by Mn^{2+} ion. In particular, the I_R/I_G ratios of these core-shell samples keep constant, which are determined as 3.25, 3.25 and 3.15 in Mn^{2+}-free, Mn^{2+}-less and Mn^{2+}-highly doped core-shell UCNPs, respectively (Fig. 4f). This indicates that the Mn^{2+} exchange in 2.5 nm shell are not able to distort the Er^{3+} site occupancy within the polyhedron structure in the core (Fig. 4g). Moreover, only interior doping leads to the efficient energy transfer between Er^{3+} and Mn^{2+}, hence the increased I_R/I_G ratio in core UCNPs testifies the successful cation exchange between Ln^{3+} and Mn^{2+} ions. The penetration depth of cation exchange within UCNPs should be less than 2.5 nm.

4. Conclusions

We have successfully achieved Mn^{2+} ions cation exchange in β-$NaYF_4$:Yb^{3+}/Er^{3+} UCNPs and observed enhanced emission intensity. We have conducted Rietveld refinement to analyse the crystal structure evolution upon exchange, and further link the crystalline analysis to spectroscopic study. For the first time, we atomically decipher the exchange process, that is, the doped Mn^{2+} replace alkaline metal (Na^+) in the lattice through $2Na^+ \leftrightarrow Mn^{2+} + Vacancy$ reaction. In the crystal system, (Na/Mn)F_6 polyhedron becomes more regular, while LnF_9 polyhedron becomes more distorted. The LnF_9 polyhedral distortion produced by Mn^{2+} addition tailored the surrounding environment around active lanthanides ions in the crystal field, thereby improving the luminescent performance of UCNPs. Further confirmed by core-shell design and spectroscopic study, we have proven that the $Mn^{2+} \leftrightarrow Na^+$ exchange enables both the emission enhancement and transition probability variation of activator ions. This suggests a new pathway to alter the symmetry of the crystal field around the activator ions, leading to enhanced upconversion luminescence.

Declaration of competing interest

There are no conflicts to declare.

CRediT authorship contribution statement

Ming Guan: Data curation, Formal analysis, Writing - original draft. **Maxim S. Molokeev:** Writing - review & editing. **Jiajia Zhou:** Supervision, Writing - review & editing.

Acknowledgements

The authors acknowledge the Science and Technology Innovation Committee of Shenzhen (Grant No. KQTD20170810110913065), Australian Research Council (ARC) Discovery Early Career Researcher Award Scheme (J. Z., DE 180100669), and the China Scholarship Council (Ming Guan, No. 201506400025).

Appendix A. Supplementary data

Supplementary data to this article can be found online at https://doi.org/10.1016/j.jlumin.2020.117289.

References

[1] J. Zhou, J.L. Leano Jr., Z. Liu, D. Jin, K.L. Wong, R.S. Liu, J.G. Bunzli, Small 14 (2018), e1801882.
[2] J. Zhou, S. Wen, J. Liao, C. Clarke, S.A. Tawfik, W. Ren, C. Mi, F. Wang, D. Jin, Nat. Photon. 12 (2018) 154–158.
[3] Y. Liu, Y. Lu, X. Yang, X. Zheng, S. Wen, F. Wang, X. Vidal, J. Zhao, D. Liu, Z. Zhou, C. Ma, J. Zhou, J.A. Piper, P. Xi, D. Jin, Nature 543 (2017) 229–233.
[4] S. Wen, J. Zhou, K. Zheng, A. Bednarkiewicz, X. Liu, D. Jin, Nat. Commun. 9 (2018) 2415.
[5] C.-W. Chen, P.-H. Lee, Y.-C. Chan, M. Hsiao, C.-H. Chen, P.C. Wu, P.R. Wu, D. P. Tsai, D. Tu, X. Chen, R.-S. Liu, J. Mater. Chem. B 3 (2015) 8293–8302.
[6] F. Zhang, G.B. Braun, A. Pallaoro, Y. Zhang, Y. Shi, D. Cui, M. Moskovits, D. Zhao, G.D. Stucky, Nano Lett. 12 (2012) 61–67.
[7] E.M. Chan, G. Han, J.D. Goldberg, D.J. Gargas, A.D. Ostrowski, P.J. Schuck, B. E. Cohen, D.J. Milliron, Nano Lett. 12 (2012) 3839–3845.
[8] X. Liu, Y. Wang, X. Li, Z. Yi, R. Deng, L. Liang, X. Xie, D.T.B. Loong, S. Song, D. Fan, A.H. All, H. Zhang, L. Huang, X. Liu, Nat. Commun. 8 (2017) 899.
[9] C. Zhang, L. Yang, J. Zhao, B. Liu, M.Y. Han, Z. Zhang, Angew Chem. Int. Ed. Engl. 54 (2015) 11531–11535.
[10] R. Arppe, T. Nareoja, S. Nylund, L. Mattsson, S. Koho, J.M. Rosenholm, T. Soukka, M. Schaferling, Nanoscale 6 (2014) 6837–6843.
[11] Y. Lu, J. Zhao, R. Zhang, Y. Liu, D. Liu, E.M. Goldys, X. Yang, P. Xi, A. Sunna, J. Lu, Y. Shi, R.C. Leif, Y. Huo, J. Shen, J.A. Piper, J.P. Robinson, D. Jin, Nat. Photon. 8 (2013) 32–36.
[12] J. Zhao, D. Jin, E.P. Schartner, Y. Lu, Y. Liu, A.V. Zvyagin, L. Zhang, J.M. Dawes, P. Xi, J.A. Piper, E.M. Goldys, T.M. Monro, Nat. Nanotechnol. 8 (2013) 729–734.
[13] Y. Zhong, Z. Ma, S. Zhu, J. Yue, M. Zhang, A.L. Antaris, J. Yuan, R. Cui, H. Wan, Y. Zhou, W. Wang, N.F. Huang, J. Luo, Z. Hu, H. Dai, Nat. Commun. 8 (2017) 737.
[14] H. He, C.B. Howard, Y. Chen, S. Wen, G. Lin, J. Zhou, K.J. Thurecht, D. Jin, Anal. Chem. 90 (2018) 3024–3029.
[15] S. Gai, P. Yang, C. Li, W. Wang, Y. Dai, N. Niu, J. Lin, Adv. Funct. Mater. 20 (2010) 1166–1172.
[16] F. Vetrone, R. Naccache, A. Juarranz de la Fuente, F. Sanz-Rodriguez, A. Blazquez-Castro, E.M. Rodriguez, D. Jaque, J.G. Sole, J.A. Capobianco, Nanoscale 2 (2010) 495–498.
[17] J. Zhou, Z. Liu, F. Li, Chem. Soc. Rev. 41 (2012) 1323–1349.
[18] W. Zheng, P. Huang, D. Tu, E. Ma, H. Zhu, X. Chen, Chem. Soc. Rev. 44 (2015) 1379–1415.
[19] G. Chen, H. Qiu, P.N. Prasad, X. Chen, Chem. Rev. 114 (2014) 5161–5214.
[20] M. Haase, H. Schafer, Angew Chem. Int. Ed. Engl. 50 (2011) 5808–5829.
[21] G.Y. Chen, H.C. Liu, G. Somesfalean, Y.Q. Sheng, H.J. Liang, Z.G. Zhang, Q. Sun, F. P. Wang, Appl. Phys. Lett. 92 (2008).
[22] Q. Cheng, J. Sui, W. Cai, Nanoscale 4 (2012) 779–784.
[23] T. Cong, Y. Ding, J. Liu, H. Zhao, X. Hong, Mater. Lett. 165 (2016) 59–62.
[24] P. Ramasamy, P. Chandra, S.W. Rhee, J. Kim, Nanoscale 5 (2013) 8711–8717.
[25] M. Liu, Y. Ye, C. Yao, W. Zhao, X. Huang, J. Mater. Chem. B 2 (2014) 6626–6633.
[26] X. Li, X. Liu, D.M. Chevrier, X. Qin, X. Xie, S. Song, H. Zhang, P. Zhang, X. Liu, Angew Chem. Int. Ed. Engl. 54 (2015) 13510–13515.
[27] G. Tian, Z. Gu, L. Zhou, W. Yin, X. Liu, L. Yan, S. Jin, W. Ren, G. Xing, S. Li, Y. Zhao, Adv. Mater. 24 (2012) 1226–1231.
[28] Z. Wu, M. Lin, S. Liang, Y. Liu, H. Zhang, B. Yang, Part. Part. Syst. Char. 30 (2013) 311–315.
[29] S. Fan, S. Wang, W. Xu, M. Li, H. Sun, L. Hu, J. Mater. Sci. 52 (2016) 869–877.
[30] M. Deng, L. Wang, Nano Research 7 (2014) 782–793.
[31] B.J. Beberwyck, Y. Surendranath, A.P. Alivisatos, J. Phys. Chem. C 117 (2013) 19759–19770.
[32] S. Han, X. Qin, Z. An, Y. Zhu, L. Liang, Y. Han, W. Huang, X. Liu, Nat. Commun. 7 (2016) 13059.
[33] D. Liu, X. Xu, Y. Du, X. Qin, Y. Zhang, C. Ma, S. Wen, W. Ren, E.M. Goldys, J. A. Piper, S. Dou, X. Liu, D. Jin, Nat. Commun. 7 (2016) 10254.
[34] K.A. Denault, J. Brgoch, M.W. Gaultois, A. Mikhailovsky, R. Petry, H. Winkler, S. P. DenBaars, R. Seshadri, Chem. Mater. 26 (2014) 2275–2282.
[35] E.-H. Song, S. Ding, M. Wu, S. Ye, F. Xiao, G.-P. Dong, Q.-Y. Zhang, J. Mater. Chem. C (2013) 1.
[36] S. Ye, Y.-j. Li, D.-c. Yu, G.-p. Dong, Q.-Y. Zhang, J. Mater. Chem. (2011) 21.